Ocean Sci. Discuss., 12, 2123–2146, 2015
www.ocean-sci-discuss.net/12/2123/2015/
doi:10.5194/osd-12-2123-2015
© Author(s) 2015. CC Attribution 3.0 License.

Ocean Science
Discussions
Open Access

This discussion paper is/has been under review for the journal Ocean Science (OS).
Please refer to the corresponding final paper in OS if available.

The near-inertial variability of meridional overturning circulation in the South China Sea as shown by an eddy-resolving ocean reanalysis

J. Xiao[1,2], D. Wang[1], Q. Xie[1,3], Y. Shu[1], C. Liu[4], and J. Chen[1]

[1]State Key Laboratory of Tropical Oceanography (LTO), South China Sea Institute of Oceanology, Chinese Academy of Sciences, Guangzhou, China
[2]University of Chinese Academy of Sciences, Beijing, China
[3]Sanya Institute of Deep-sea Science and Engineering, Chinese Academy of Sciences, Sanya, China
[4]South China Sea Marine Engineering Survey Center, State Ocean Administration, Guangzhou, China

Received: 21 July 2015 – Accepted: 26 August 2015 – Published: 10 September 2015

Correspondence to: D. Wang (dxwang@scsio.ac.cn)

Published by Copernicus Publications on behalf of the European Geosciences Union.

Abstract

The near-inertial variability of the meridional overturning circulation in the South China Sea (SCSMOC) has been analyzed based on a global 1/12° ocean reanalysis. The wavelet analysis and power spectrum of deep SCSMOC time series shows that there is a significant signal in the near-inertial band. The maximum amplitude of the near-inertial signal in the SCSMOC is nearly 4 Sv. The spatial structure of the signal features regularly alternating counterclockwise and clockwise overturning cells. It is also found that the near-inertial signal of SCSMOC mainly originates from the Luzon Strait and propagates equatorward with the speed of 1–3 m s^{-1}. Further analyses suggest that the near-inertial signal in the SCSMOC is triggered by high-frequency wind variability near the Luzon Strait where geostrophic shear always exists due to Kuroshio intrusion.

1 Introduction

The widest and deepest channel in the South China Sea (SCS) is the Luzon Strait, which has a sill depth of about 2400 m and is the main passage between the SCS and the northwestern Pacific Ocean (Qu et al., 2006). Previous studies show that the SCS acts as a mixing mill that mixes the surface and deep waters and returns the mixed waters to the Luzon Strait at an intermediate depth (Yuan, 2002; Tian et al., 2009; Yang et al., 2013, 2014). Based on field observations, studies confirm the hypothesis that the Luzon Strait transport (LST) has a sandwiched vertical structure, which shows a westward flow in the upper layer (< 500 m) and in the deeper layer (> 1500 m), and an eastward flow in the intermediate layer (500–1500 m) (Tian et al., 2006; Yang et al., 2010). The corresponding circulation in the SCS is consistent with the Stommel and Arons theory (Stommel et al., 1960a and b), which suggests that the mixing-induced circulation inside the SCS should be cyclonic gyres at the surface and at the bottom (Chao et al., 1996; Li et al., 2006; Wang et al., 2011; Lan et al., 2013; Xu et al., 2014), and an anti-cyclonic gyre at an intermediate depth (Isobe et al., 2001; Yuan, 2002).

OSD
12, 2123–2146, 2015

Note that the upper-layer SCS circulation is also affected by the seasonally reversing monsoon, exhibiting a cyclonic circulation over the whole SCS basin in winter and in summer a strong anti-cyclonic circulation in the southern SCS and a weak cyclonic circulation in the northern SCS (Wrytki, 1961; Chu et al., 1999; Chu and Li, 2000; Qu, 2000; Hu et al., 2000; Liu et al., 2001; Wang et al., 2003; Su, 2004).

In the context of the strong mixing in the SCS and the sandwiched vertical structure of the Luzon Strait transport, Wang et al. (2004) proposed that the shallow meridional overturning in the SCS (SCSMOC) is non-enclosed, transporting waters from north to south at the depth of about 500 m (200 m) and returning waters to north at surface in winter (summer). The shallow SCSMOC hints at a transport path such that intermediate water enters the SCS from the northwestern Pacific (Wang et al., 2004; Xie et al., 2013). Zhang et al. (2014) further show that the shallow SCSMOC consists of downwelling in the northern SCS, a southward subsurface branch supplying upwelling in the southern SCS and a northward return flow of surface water. Based on the high-resolution global reanalysis data (GLBa0.08), Shu et al. (2014) found that the whole SCSMOC also has a sandwiched structure driven by the Luzon Strait transport, consisting of a stronger non-enclosed clockwise overturning circulation in the upper layer, a weaker counterclockwise overturning circulation in the intermediate layer, and a weaker clockwise overturning circulation in the deep layer.

The SCSMOC variability spans a wide range of time scales. On a decadal time scale, the intermediate water of the SCS was fresher in the 1980s than that in the 1960s, caused by the deep SCSMOC decreasing from the 1960s to the 1980s according to an ocean reanalysis (Liu et al., 2012). On the interannual scale, the Luzon Strait transport shows a remarkable inter-annual variability associated with El Niño-Southern Oscillation (ENSO) (Qu et al., 2004). The upper LST correlates with the local wind stress while the lower LST shows a statistically significant correlation with Niño3.4 index (Qu et al., 2005; Wang, D. et al., 2006; Wang, Y. et al., 2006), indicating that the shallow SCSMOC also has an interannual variability related with ENSO. On a seasonal scale, the seasonal variability of the shallow SCSMOC mostly controls the strength of sea-

OSD
12, 2123–2146, 2015

sonal intrusions of the North Pacific Water into the SCS (Liu et al., 2008). Moreover, the deep overflow through the Luzon Strait is strong in summer while weak in winter, driving the seasonal variability of the deep SCSMOC (Lan et al., 2015). However, there is no study so far for shorter time-scale (several days) variability of the SCSMOC.

The existence of near-inertial (several days) variability of the Atlantic meridional Ocean circulation (AMOC) has been recently reported by using a high-resolution oceanic general circulation model (Blaker et al., 2012). This variability is associated with equatorward-propagating near-inertial gravity waves (NIGWs). Whether high frequency (near-inertial) variability exists in the SCSMOC is the main purpose of this study. The rest of the paper is organized as follows. The data and methods are introduced in Sect. 2. The results are presented in Sect. 3. Sections 4 and 5 give discussion and conclusion.

2 Data and method

The product of Hybrid Coordinate Ocean Model + Navy Coupled Ocean Data Assimilation (HYCOM + NCODA) global 1/12° Reanalysis (GLBu0.08, http://hycom.org/dataserver/glb-reanalysis) provided by the Naval Research Laboratory is used in this study. As a dynamical model, HYCOM 2.2 is configured for the global ocean with the bathymetry derived from the 30 arc-second GEBCO (General Bathymetric Chart of the Oceans) dataset. The K-Profile Parameterization (KPP) mixing scheme is adopted for the vertical diffusion of momentum, temperature, and salinity (Thoppil et al., 2011). The model is forced by the hourly wind stress and heat fluxes derived from National Center for Environmental Prediction (NCEP) Climate Forecast System Reanalysis (CFSR) with horizontal resolution of 0.3125°. Note that there is no tidal forcing during the integration. It is initialized using temperature and salinity from the 1/4° Generalized Digital Environmental Model (GDEM4) climatology in January. The NCODA assimilates available satellite altimeter observations, satellite and in-situ sea surface temperature (SST) as well as available in-situ vertical temperature and salinity profiles from XBTs, Argo

OSD
12, 2123–2146, 2015

floats and moored buoys using a 3-D variational scheme (Cummings, 2005). The model output is stored every 3 h.

Based on the equation of continuity, the meridional overturning streamfunction can be defined as

$$\frac{\partial \psi(y,z,t)}{\partial z} = \int_{x_e}^{x_w} v(x,y,z,t)\mathrm{d}x \quad (1)$$

$$\frac{\partial \psi(y,z,t)}{\partial y} = -\int_{x_e}^{x_w} w(x,y,z,t)\mathrm{d}x \quad (2)$$

Because there is no vertical velocity (w) provided in GLBu0.08, the meridional overturning streamfunction in SCS could be calculated as:

$$\psi(y,z,t) = \int_{-H}^{z} \mathrm{d}z \int_{x_e}^{x_w} v(x,y,z,t)\mathrm{d}x, \quad (3)$$

where x_w and x_e are the western and eastern limits of the basin, respectively, and H is the ocean bottom. Although the meridional overturning streamfunction is calculated only by the meridional velocity (v), it also represents the integrated vertical motions in the basin because of the equation of continuity (Endoh et al., 2007). Shu et al. (2014) have used another product of HYCOM + NCODA global 1/12° Reanalysis (GLBa0.08, Fig. 1a) to depict the structure of the SCSMOC. The only difference between GLBa0.08 and GLBu0.08 is the external forcing field. GLBa0.08 is forced by Navy Operational Global Atmospheric Prediction System (NOGAPS), while GLBu0.08 is driven by Climate Forecast System Reanalysis (CFSR). Figure 1 shows the SCS meridional overturning stream function averaged from 2004 to 2010 based on GLBa0.08 and GLBu0.08. It is found that the two products show a roughly similar SC-

OSD
12, 2123–2146, 2015

SMOC, which consists of a non-enclosed clockwise upper overturning cell, a counter-clockwise intermediate overturning cell and a clockwise deep overturning cell as shown in Fig. 1. The main difference is that the intermediate cell in GLBu0.08 is stronger and the deep cell stretches less southward compared with the GLBa0.08. And the upper cell in GLBu0.08 is deeper. More importantly, compared with the daily-output GLBa0.08, GLBu0.08 has a three-hour output, which is better for studying motion with periods of only a few days. So the GLBu0.08 product in 2010 is chosen to analyze the characteristics of near-inertial variability of the SCSMOC in this study.

3 Characteristics of the near-inertial variability of the SCSMOC

Figure 2a shows the 120-day time series of the deep SCSMOC (at 1500 m and 14° N) in 2010. It is found that the SCSMOC experiences an obvious intra-seasonal variability superimposed with persistent high-frequency undulations (Fig. 2a). The wavelet analysis shows that the high-frequency undulations are corresponding to strong and persistent power in the band of 1–3 days while the intra-seasonal variability has power with periods of about 16–32 days (Fig. 2b). The spectral analysis further confirms that there is an obvious period band of 1–3 days in the deep SCSMOC time series (Fig. 2c). It is also found that the period corresponding to the power peak of SCSMOC is prolonged equatorward from 1 day at 20° N to 3 days at 10° N (Fig. 3a). It is noted that the near-inertial band in the SCS is from 1.46 days at 20° N to 3.59 days at 10° N (Chen et al., 2014). Comparing with the local inertial period in the SCS, the deep SCSMOC is at sub-inertial periods, while the shallow SCSMOC is at inertial periods. However, the SCSMOC between 8 and 10° N is at super-inertial periods.

To extract the near-inertial signal of the SCSMOC, a third-order Butterworth filter is applied to the time series of the SCSMOC at each latitude and depth. Cutoff frequencies are set at [0.33, 1] cpd, which is corresponding to the 1–3 day band. The maximum standard deviation (SD) of the filtered SCSMOC signal is nearly 4 Sv (Fig. 4b), which is nearly half of the maximum SD of total SCSMOC in 2010 (Fig. 4a). The largest

OSD
12, 2123–2146, 2015

amplitude of the near-inertial signal in SCSMOC is found in mid layer (500–2500 m). There are two high SDs at mid depth (500–2500 m), the northern one is between 16 and 20° N, and the southern one is between 12 and 14° N (Fig. 4b). Near Luzon Strait (around 19° N in Fig. 4b) exists a maximum of the shallow SCSMOC variability in the layer (100–500 m).

Based on the snapshot of the integrated filtered meridional velocity field from the bottom to 1000 m at 24:00, 15 January 2010 (Fig. 5a), it is obvious that the integrated velocity field consists of regularly alternating positive and negative bands. Furthermore, Fig. 5b is the snapshot of the filtered SCSMOC signal at the same time as in Fig. 5a. The spatial structure of the near inertial signal is stacked with regularly alternating positive and negative cells. The maximum amplitude of these cells is nearly 5 Sv, and most of the cells concentrate in the depth between 1000 to 2500 m and within the latitude between 10 and 20° N while the cells are not so evident in the upper layer. These cells are not stretched in the meridional direction but in the vertical direction which means each cell consists of the strong upwelling branch and downwelling branch. From 4 to 10° N and 20 to 22° N, there are also weak cells. The upwelling and downwelling in the mid depths are also found in the open ocean like the Atlantic and Pacific Ocean based on the high-resolution model simulations where the vertical velocity was used to diagnose the deep ocean near-inertial gravity waves (Komori et al., 2008; von Storch, 2010). The pattern of the near-inertial variability of SCSMOC (Fig. 4b) is very similar to the near-inertial variability of the Pacific Ocean or Atlantic. And the period corresponding to the power peak of the AMOC is mostly at near inertial periods (Komori et al., 2008), which indicates that the near-inertial signal of the SCSMOC is not unique in nature.

To investigate the meridional propagation of near-inertial signals in the SCSMOC in mid-depths (500–2500 m), Fig. 6 shows the meridional structure of the filtered near-inertial signal at 1500 m in four typical months (January, April, July and October) in 2010. It is found that most of the signal propagates from 18° N (the latitude of the southern tip of the Luzon Strait) regardless of the different months. The propagating

OSD
12, 2123–2146, 2015

velocity is estimated as about 1–3 m s^{-1}. It was noted that the NIGWs usually have the dominant frequency of f (Coriolis frequency) and usually propagate equatorward due to beta-dispersion (Anderson and Gill, 1979; Nagasawa et al., 2000; Garrett, 2001). The meridional propagation of the filtered SCSMOC signal and near inertial period (Fig. 3b) indicate that the striped pattern of the filtered 1–3 day SCSMOC signal represents ocean NIGWs formed especially near the Luzon Strait and propagating equatorward.

4 Discussion

The SCS is affected by the East Asian monsoon system and frequently experiences strong tropical cyclones originating from the western Pacific (Zheng et al., 2015). Strong vertical mixing and horizontal pressure gradients caused by typhoon winds can lead to the formation of strong NIGWs in the ocean interior (Garrett, 2001). Previous observations of NIGWs are focused on the upper layer in the SCS (Liang et al., 2005; Xie et al., 2009; Xu et al., 2013; Chen et al., 2013), only Yuan et al. (2002) have found there are strong NIGWs below 1800 m in the northeastern SCS using two current-meters. Our mooring was located at 114.57° E, 17.99° N, where the water depth is about 3500 m. An Aanderaa current-meter was positioned at 300 m above the bottom and the valid current-meter data were collected from 21 March to 19 September 2006 with the sampling interval of 1 h. The 120-day data since April 1, 2006 was used in this study. The power spectrum of zonal velocity and meridional velocity clearly peaks at the inertial frequency (Fig. 7).

The imprint of NIGWs on AMOC has been found mostly related to wintertime storm tracks (Blaker et al., 2012; Sévellec et al., 2013; Furuichi et al., 2013; Rimac et al., 2013). However, the imprint of NIGWs on SCSMOC might be related to wind variability near Luzon Strait (Li et al., 2015). Figure 8 further shows the monthly mean near-inertial energy input by wind during four typical months (January, April, July and October) in 2010. It is found that wind-induced near-inertial energy input is always strong west of the Luzon Strait. In spring, autumn and winter, these strong high-frequency

OSD
12, 2123–2146, 2015

wind wakes in the Luzon Strait could drive the NIGWs near the Luzon Strait (Fig. 8a–b and d). An average of about 7 TCs pass through the Luzon Strait from the Northwest Pacific Ocean each year (Wang et al., 2007; Zheng et al., 2015), inducing strong wind-induced near-inertial energy input into the ocean (Fig. 8c), so TCs could also be drivers of the NIGWs near the Luzon Strait. The horizontal distribution of large integrated near-inertial kinetic energy roughly corresponds to that of the strong wind-induced near-inertial energy input (Figs. 8 and 9). Additionally, due to beta-dispersion of the NIGWs (Anderson and Gill, 1979; Garrett, 2001), the region of the integrated near-inertial kinetic energy is stretched equatorward. Furthermore, a strong density front usually exists in the Luzon strait due to the Kuroshio (Wang et al., 2001), inducing positive vorticity west of the Kuroshio and negative vorticity to its east. On the one hand, the disturbance of the front (Kuroshio) can drive NIGWs through geostrophic adjustment (Kunze, 1985; Wang et al., 2009; Whitt et al., 2013). On the other hand, the transfer of near-inertial energy to the deep ocean can be enhanced by the negative vorticity field (Lee et al., 1997; Zhai et al., 2005). As the NIGWs leave the density front, they will propagate equatorward due to beta-dispersion (Anderson and Gill, 1979; Garrett, 2001). Therefore, strong NIGWs near the Luzon Strait can be detected in the deep SCSMOC south of the Luzon Strait as far as 10° N.

5 Conclusions

A high-resolution ocean reanalysis (GLBu0.08) is used to depict the characteristics of the near-inertial variability in the deep SCSMOC. It is shown that there is an obvious high power peak in the 1–3 day band in the deep SCSMOC time series, which is in the near-inertial band in the SCS. The maximum amplitude of the near-inertial signal in the SCSMOC is nearly 4 Sv. The large amplitude of the near-inertial signal in SCSMOC is found in mid layer (500–2500 m) .The near-inertial signal in SCSMOC propagates equatorward with the speed of 1–3 $m\,s^{-1}$ from the Luzon Strait. The imprint of NIGWs on the SCSMOC highlights the possible importance of NIGWs in the horizontal and

OSD
12, 2123–2146, 2015

vertical redistribution of wind energy throughout the SCS. Although the effect of these NIGWs in depth on turbulent mixing is still unknown, however, it is speculated that the breaking of these deep ocean NIGWs could be a candidate for the enhanced mixing in the SCS.

Acknowledgements. This work was supported by the National Basic Research Program of China (91228202 and 41276024), the Knowledge Innovation Engineering Frontier Project of Sanya Institute of Deep Sea Science and Engineering (SIDSSE-201205), Sanya and Chinese Academy of Sciences Cooperation Project (2012YD01) and Strategic Priority Research Program of the Chinese Academy of Sciences (XDB06020102).

References

Anderson, D. L. T. and Gill, A. E.: Beta dispersion of inertial waves, J. Geophys. Res.-Oceans, 84, 1836–1842, 1979.

Blaker, A. T., Hirschi, J. J. M., Sinha, B., de Cuevas, B., Alderson, S., Coward, A., and Madec, G.: Large near-inertial oscillations of the Atlantic meridional overturning circulation, Ocean Model., 42, 50–56, 2012.

Chao, S. Y., Shaw, P. T., and Wu, S. Y.: Deep water ventilation in the South China Sea, Deep-Sea Res. Pt. I, 43, 445–466, 1996.

Chen, G., Xue, H., Wang, D., and Xie, Q.: Observed near-inertial kinetic energy in the northwestern South China Sea, J. Geophys. Res.-Oceans, 118, 4965–4977, doi:10.1002/jgrc.20371, 2013.

Chiswell, S. M.: Deep equatorward propagation of inertial oscillations, Geophys. Res. Lett., 30, 1533, doi:10.1029/2003GL017057, 2003.

Chu, P. C. and Li, R.: South China Sea isopycnal-surface circulation, J. Phys. Oceanogr., 30, 2419–2438, 2000.

Chu, P. C., Edmons, N. L., and Fan, C. W.: Dynamical mechanisms for the South China Sea seasonal circulation and thermohaline variabilities, J. Phys. Oceanogr., 29, 2971–2989, 1999.

Cummings, J. A.: Operational multivariate ocean data assimilation, Q. J. Roy. Meteor. Soc., 131, 3583–3604, 2005.

OSD
12, 2123–2146, 2015

Endoh, T. and Hibiya, T.: Meridional overturning circulation of the deep Pacific estimated assuming the vertical advective-diffusive balance, Geophys. Res. Lett., 34, L11602, doi:10.1029/2007GL030027, 2007.
Fang, G., Wang, Y., Wei, Z., Fang, Y., Qiao, F., and Hu, X.: Interocean circulation and heat and freshwater budgets of the South China Sea based on a numerical model, Dynam. Atmos. Oceans, 47, 55–72, 2009.
Furuichi, N., Hibiya, T., and Niwa, Y.: Model-predicted distribution of wind-induced internal wave energy in the world's oceans, J. Geophys. Res.-Oceans, 113, C09034, doi:10.1029/2008JC004768, 2008.
Garrett, C.: What is the "near-inertial" band and why is it different from the rest of the internal wave spectrum?, J. Phys. Oceanogr., 31, 962–971, 2001.
Hu, J. Y., Kawamura, H., Hong, H. S., and Qi, Y.: A review on the currents in the South China Sea: Seasonal circulation, South China Sea Warm Current and Kuroshio intrusion, J. Oceanogr., 56, 607–624, 2000.
Isobe, A. and Namba, T.: The circulation in the upper and intermediate layers of the South China Sea, J. Oceanogr., 57, 93–104, 2001.
Komori, N., Ohfuchi, W., Taguchi, B., Sasaki, H., and Klein, P.: Deep ocean inertia-gravity waves simulated in a high-resolution global coupled atmosphere–ocean GCM, Geophys. Res. Lett., 35, L04610, doi:10.1029/2007GL032807, 2008.
Kunze, E.: Near-inertial wave propagation in geostrophic shear, J. Phys. Oceanogr., 15, 544–565, 1985.
Lan, J., Zhang, N., and Wang, Y.: On the dynamics of the South China Sea deep circulation, J. Geophys. Res.-Oceans, 118, 1206–1210, 2013.
Lan, J., Wang, Y., Cui, F., and Zhang, N.: Seasonal variation in the South China Sea deep circulation, J. Geophys. Res.-Oceans, 120, 1682–1690, 2015.
Lee, D. K. and Niiler, P. P.: The inertial chimney: The near-inertial energy drainage from the ocean surface to the deep layer, J. Geophys. Res., 103, 7579–7591, 1998.
Liang, X. F., Zhang, X. Q., and Tian, J. W.: Observation of internal tides and near-inertial motions in the upper 450 m layer of the northern South China Sea, Chinese Sci. Bull., 50, 2890–2895, 2005.
Li, J., Liu, J., Cai, S., and Pan, J.: The spatiotemporal variation of the wind-induced near-inertial energy flux in the mixed layer of the South China Sea, Acta Oceanol. Sin., 34, 66–72, 2015

OSD
12, 2123–2146, 2015

Li, L. and Qu, T.: Thermohaline circulation in the deep South China Sea basin inferred from oxygen distributions, J. Geophys. Res.-Oceans, 111, C05017, doi:10.1029/2005JC003164, 2006.

Liu, C., Wang, D., Chen, J., Du, Y., and Xie, Q.: Freshening of the intermediate water of the South China Sea between the 1960s and the 1980s, Chin. J. Oceanol. Limn.,30, 1010–1015, 2012.

Liu, C. J., Du, Y., Zhang, Q. R., and Wang, D. X.: Seasonal variation of subsurface and intermediate water masses in the South China Sea, Oceanologia et Limnologia Sinica, 39, 55–64, 2008.

Liu, Q., Yang, H., and Liu, Z.: Seasonal features of the Sverdrup circulation in the South China Sea, Prog. Nat. Sci., 11, 202–206, 2001.

Qu, T., Kim, Y. Y., Yaremchuk, M., Tozuka, T., Ishida, A., and Yamagata, T.: Can Luzon Strait transport play a role in conveying the impact of ENSO to the South China Sea?, J. Clim., 17, 3644–3657, 2004.

Qu, T., Du, Y., Meyers, G., Ishida, A., and Wang, D.: Connecting the tropical Pacific with Indian Ocean through South China Sea, Geophys. Res. Lett., 32, L24609, doi:10.1029/2005GL024698, 2005.

Qu, T., Girton, J. B., and Whitehead, J. A.: Deepwater overflow through Luzon strait, J. Geophys. Res.-Oceans, 111, C01002, doi:10.1029/2005JC003139, 2006.

Qu, T. D.: Upper-layer circulation in the South China Sea, J. Phys. Oceanogr., 30, 1450–1460, 2000.

Rimac, A., von Storch, J.-S., Eden, C., and Haak, H.: The influence of high-resolution wind stress field on the power input to near-inertial motions in the ocean, Geophys. Res. Lett., 40, 4882–4886, doi:10.1002/grl.50929, 2013.

Sévellec, F., Hirschi, J. J. M., and Blaker, A. T.: On the Near-Inertial Resonance of the Atlantic Meridional Overturning Circulation, J. Phys. Oceanogr., 43, 2661–2672, 2013.

Shu, Y., Xue, H., Wang, D., Chai, F., Xie, Q., Yao, J., and Xiao, J.: Meridional overturning circulation in the South China Sea envisioned from the high-resolution global reanalysis data GLBa0.08, J. Geophys. Res.-Oceans, 119, 3012–3028, 2014.

Stommel, H. and Arons, A. B.: On the abyssal circulation of the world ocean–I. Stationary flow patterns on a sphere, Deep-Sea Res. Pt. I, 6, 140–154, 1960a.

OSD
12, 2123–2146, 2015

Stommel, H. and Arons, A. B.: On the abyssal circulation of the world ocean–II. An idealized model of the circulation pattern and amplitude in oceanic basins, Deep-Sea Res. Pt. I, 6, 217–233, 1960b.
Su, J.: Overview of the South China Sea circulation and its influence on the coastal physical oceanography outside the Pearl River Estuary, Cont. Shelf Res., 24, 1745–1760, 2004.
Thoppil, P. G., Richman, J. G., and Hogan, P. J.: Energetics of a global ocean circulation model compared to observations, Geophys. Res. Lett., 38, L15607, doi:10.1029/2011GL048347, 2011.
Tian, J., Yang, Q., Liang, X., Xie, L., Hu, D., Wang, F., and Qu, T.: Observation of Luzon Strait transport, Geophys. Res. Lett., 33, L19607, doi:10.1029/2006GL026272, 2006.
Tian, J., Yang, Q., and Zhao, W.: Enhanced diapycnal mixing in the South China Sea, J. Phys. Oceanogr., 39, 3191–3203, 2009.
von Storch, J.-S.: Variations of vertical velocity in the deep oceans simulated by a 1/10° OGCM, Ocean Dynam., 60, 759–770, 2010.
Wang, D., Liu, Y., Qi, Y., and Shi, P.: Seasonal variability of thermal fronts in the northern South China Sea from satellite data, Geophys. Res. Lett., 28, 3963–3966, 2001.
Wang, D., Liu, X., Wang, W., Du, Y., and Zhou, W.: Simulation of meridional overturning in the upper layer of the South China Sea with an idealized bottom topography, Chinese Sci. Bull., 49, 740–747, 2004.
Wang, D., Liu, Q., Huang, R. X., Du, Y., and Qu, T.:Interannual variability of the South China Sea throughflow inferred from wind data and an ocean data assimilation product, Geophys. Res. Lett., 33, L14605, doi:10.1029/2006GL026316, 2006.
Wang, G., Su, J., Ding ,Y., and Chen, D.: Tropical cyclone genesis over the south China sea, J. Marine Syst., 68, 318–326, 2007.
Wang, G., Xie, S. P., Qu, T., and Huang, R. X.: Deep South China Sea circulation, Geophys. Res. Lett., 38, L05601, doi:10.1029/2010GL046626,2011.
Wang, S., Zhang, F., and Snyder, C.: Generation and propagation of inertia-gravity waves from vortex dipoles and jets, J. Atmos. Sci, 66, 1294–1314, 2009.
Wang, W., Wang, D., Shi, P., Guo, P., and Gan, Z.: Establishment and adjustment of monsoon-driven circulation in the South China Sea, Sci. China Ser. D, 46, 173–181, 2003a.
Wang, Y., Fang, G., Wei, Z., Qiao, F., and Chen, H.: Interannual variation of the South China Sea circulation and its relation to El Niño, as seen from a variable grid global ocean model, J. Geophys. Res.-Oceans, 111, C11S14, doi:10.1029/2005JC003269, 2006.

OSD
12, 2123–2146, 2015

Whitt, D. B. and Thomas, L. N.: Near-inertial waves in strongly baroclinic currents, J. Phys. Oceanogr., 43, 706–725, 2013.
Wyrtki, K.: Physical oceanography of the southeast Asian waters: Scientific results of marine investigations of the South China Sea and the Gulf of Thailand 1959–1961, NAGA Rep. 2, 195 pp., Scripps Inst. of Oceanogr., La Jolla, CA, USA, 1961.
Xie, Q., Xiao, J. G., Wang, D. X., and Yu, Y. Q.: Analysis of deep-layer and bottom circulations in the South China Sea based on eight quasi-global ocean model outputs, Chinese Sci. Bull., 58, 4000–4011, 2013.
Xie, X.-H., Shang, X.-D., Chen, G.-Y., and Sun, L.: Variations of diurnal and inertial spectral peaks near the bi-diurnal critical latitude, Geophys. Res. Lett., 36, L02606, doi:10.1029/2008GL036383, 2009.
Xu, F. H. and Oey, L. Y.: State analysis using the Local Ensemble Transform Kalman Filter (LETKF) and the three-layer circulation structure of the Luzon Strait and the South China Sea, Ocean. Dynam., 64, 905–923, 2014.
Xu, Z., Yin, B., Hou, Y., and Xu, Y.: Variability of internal tides and near-inertial waves on the continental slope of the northwestern South China Sea, J. Geophys. Res.-Oceans, 118, 197–211, doi:10.1029/2012JC008212, 2013.
Yang, Q., Tian, J., and Zhao, W.: Observation of Luzon Strait transport in summer 2007, Deep-Sea Res. Pt. I, 57, 670–676, 2010.
Yang, Q., Zhou, L., Tian, J., and Zhao, W.: The Roles of Kuroshio Intrusion and Mesoscale Eddy in Upper Mixing in the Northern South China Sea, J. Coastal. Res, 30, 192–198, 2013.
Yang, Q., Tian, J., Zhao, W., Liang, X., and Zhou, L.: Observations of turbulence on the shelf and slope of northern South China Sea, Deep-Sea Res. Pt. I, 87, 43–52, 2014.
Yuan, D.: A numerical study of the South China Sea deep circulation and its relation to the Luzon Strait transport, Acta Oceanol. Sin., 21, 187–202, 2002.
Yuan, Y. C., Zhao, J. P., Wang, H. Q., Lou, R. Y., Chen, H., and Wang, K. S.: The observation and spectral analysis of currents above 450 and in the deep depth of the northeastern South China Sea, Sci. China Earth Sci., 32, 163–176, 2002.
Zhai, X., Greatbatch, R. J., and Zhao, J.: Enhanced vertical propagation of storm-induced near-inertial energy in an eddying ocean channel model, Geophys. Res. Lett., 32, L18602, doi:10.1029/2005GL023643, 2005.
Zhang, N., Lan, J., and Cui, F.: The shallow meridional overturning circulation of the South China Sea, Ocean Sci. Discuss., 11, 1191–1212, doi:10.5194/osd-11-1191-2014, 2014.

OSD
12, 2123–2146, 2015

Zheng, L., Wang, G., and Wang, C.: Out-of-phase relationship between tropical cyclones generated locally in the South China Sea and non-locally from the Northwest Pacific Ocean, Clim. Dynam., 45, 1129–1136, 2015.

OSD
12, 2123–2146, 2015

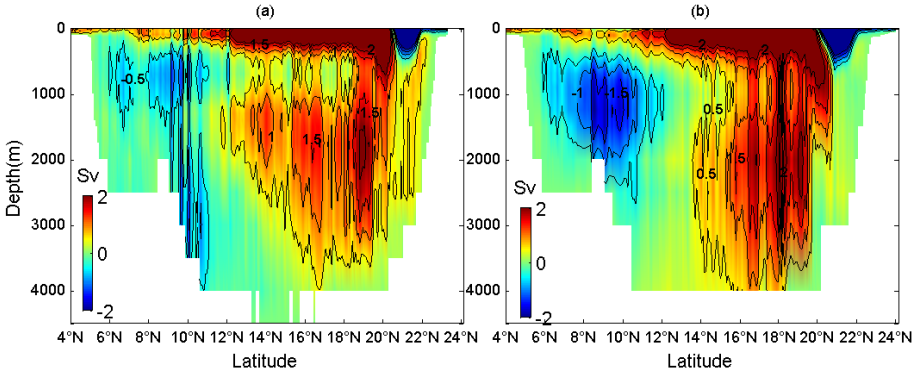

Figure 1. SCSMOC averaged from 2004 to 2010 based on GLBa0.08 **(a)** and GLBu0.08 **(b)**.

OSD
12, 2123–2146, 2015

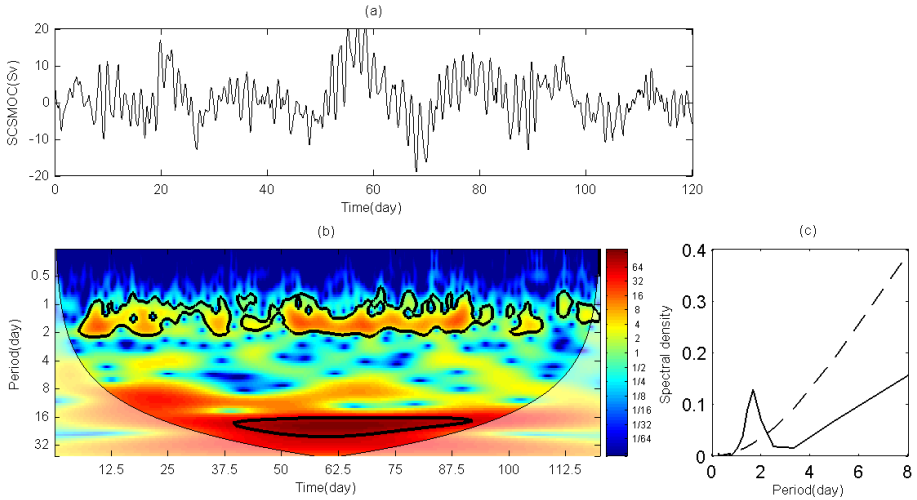

Figure 2. (a) The time series of SCSMOC at 1500 m, 14° N; **(b)** The continuous wavelet power spectrum (black contours representing 95 % significance); **(c)** The power spectrum (dashed line showing 95 % confidence levels).

OSD
12, 2123–2146, 2015

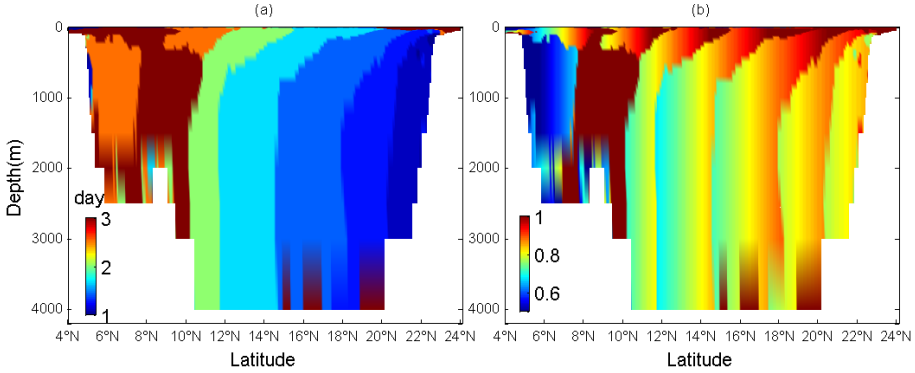

Figure 3. (a) The period corresponding to the power peak of the SCSMOC, which passes 95 % significance; **(b)** The ratio of the peak period of the SCSMOC to the local inertial period.

OSD
12, 2123–2146, 2015

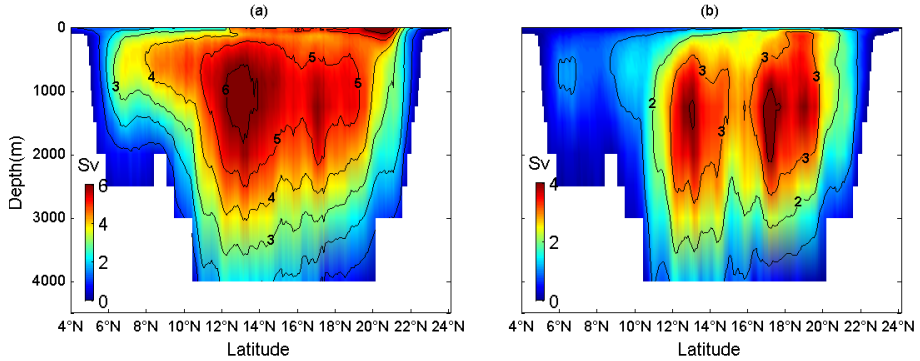

Figure 4. (a) The SDs of the SCSMOC in 2010and **(b)** The filtered 1–3 day SCSMOC signal in 2010.

OSD
12, 2123–2146, 2015

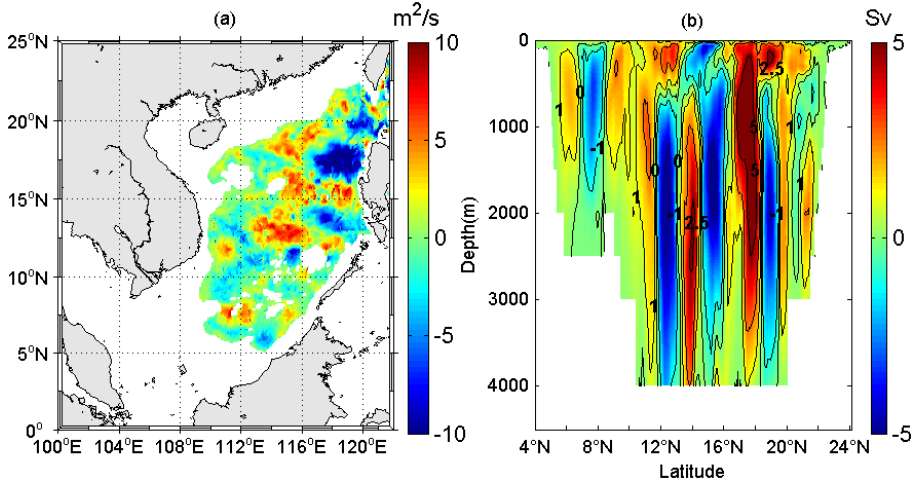

Figure 5. The snapshot of **(a)** the integrated velocity field from the bottom to 1000 m and **(b)** the filtered SCSMOC signal at 24:00, January 2010.

OSD
12, 2123–2146, 2015

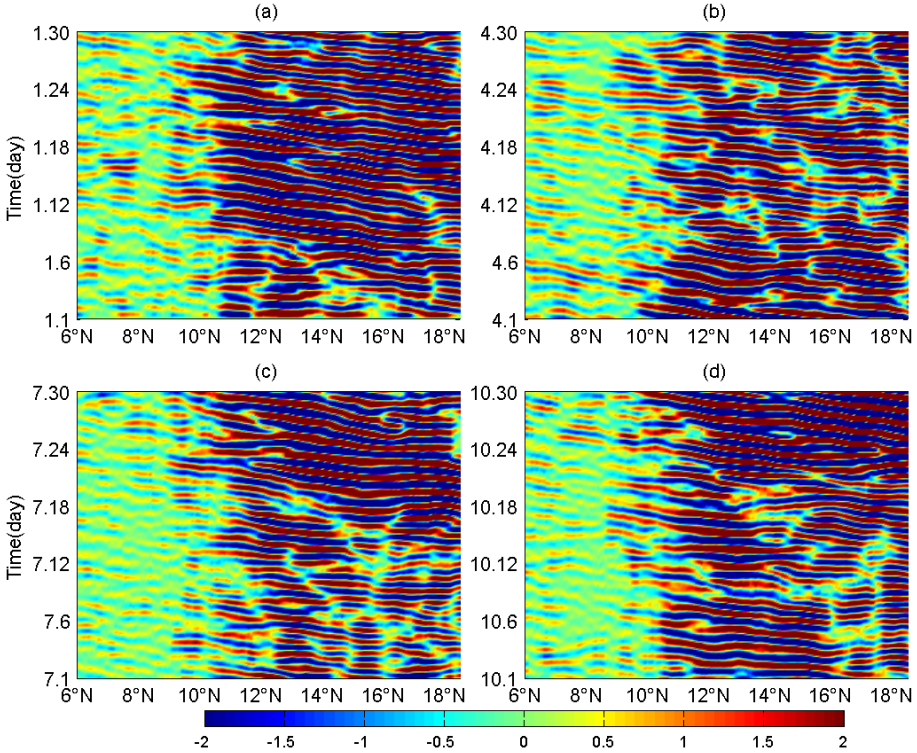

Figure 6. Time-latitude plot of 1–3 day band-passed SCSMOC signal at 1500 m in **(a)** January, **(b)** April, **(c)** July and **(d)** October in 2010.

OSD
12, 2123–2146, 2015

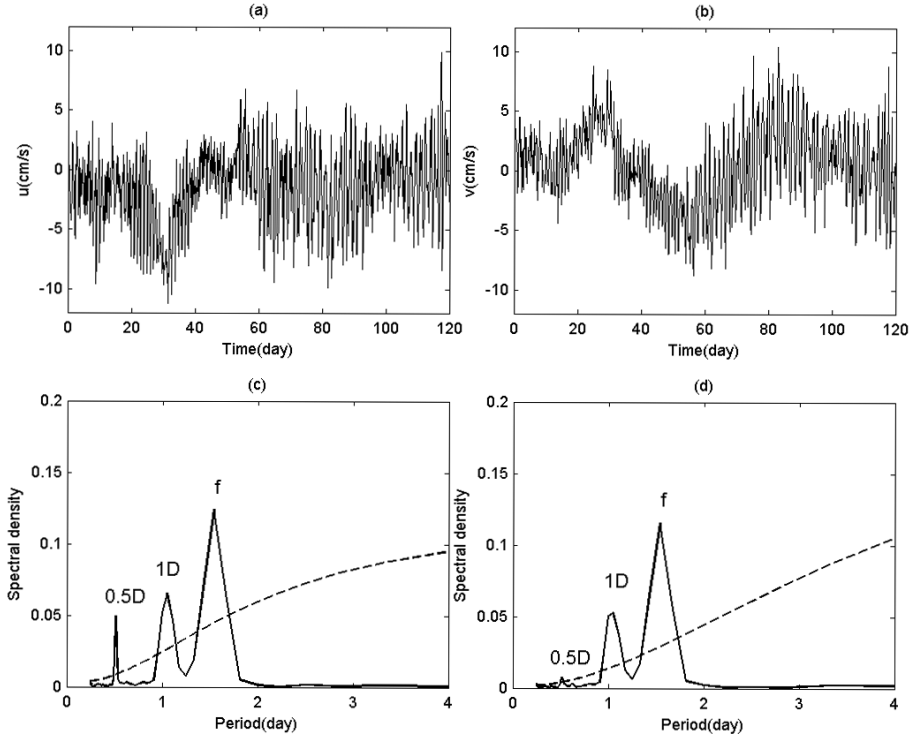

Figure 7. The time series of zonal velocity **(a)** and its power spectrum **(c)**; and the time series of meridional velocity **(b)** and its power spectrum **(d)**. The dashed line shows 95 % confidence levels.

OSD
12, 2123–2146, 2015

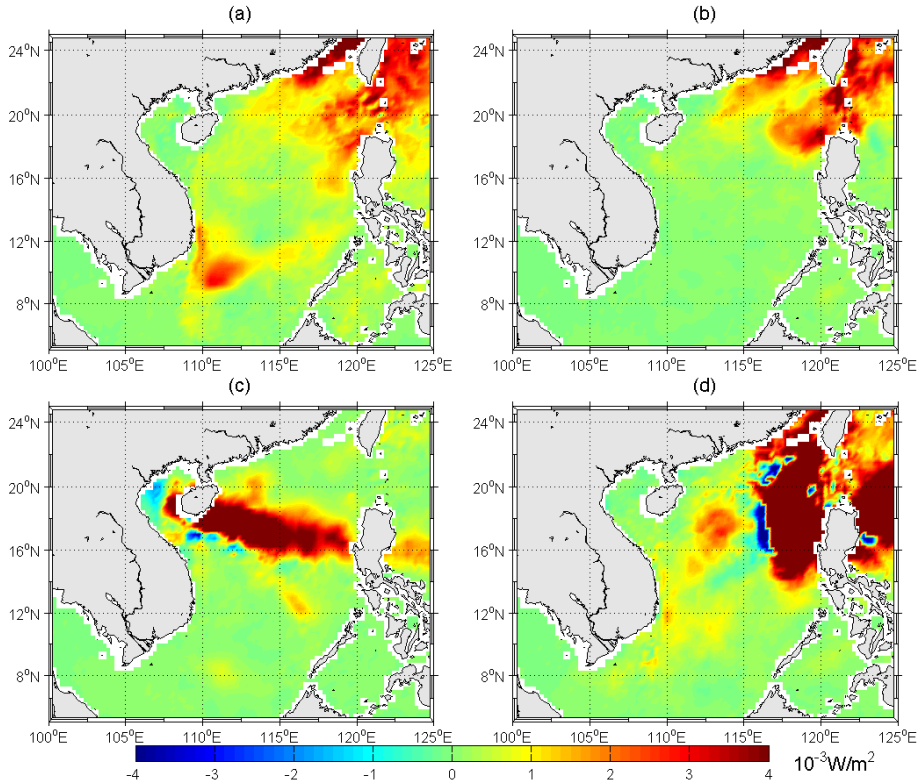

Figure 8. Spatial distribution of the monthly mean near-inertial energy input by wind in **(a)** January, **(b)** April, **(c)** July and **(d)** October in 2010.

OSD
12, 2123–2146, 2015

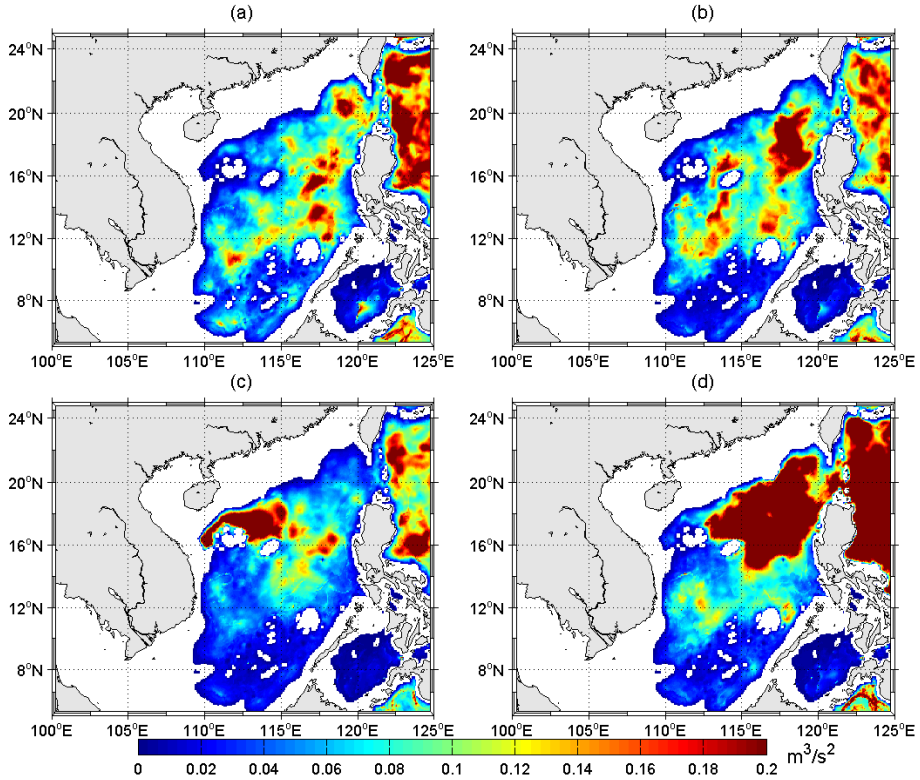

Figure 9. The monthly mean integrated near-inertial kinetic energy from the bottom to 1000 m in **(a)** January, **(b)** April, **(c)** July and **(d)** October in 2010.

OSD
12, 2123–2146, 2015